J Nanopart Res (2013) 15:1658
DOI 10.1007/s11051-013-1658-6

RESEARCH PAPER

A new function of graphene oxide emerges: inactivating phytopathogenic bacterium *Xanthomonas oryzae pv. Oryzae*

Juanni Chen · Xiuping Wang · Heyou Han

Received: 18 January 2013 / Accepted: 14 April 2013 / Published online: 30 April 2013

Abstract *Xanthomonas oryzae pv. oryzae* (*Xoo*) is one representative phytopathogenic bacterium causing bacteria infections in rice. The antibacterial activity of graphene suspended in different dispersants against *Xoo* was first investigated. Bacteriological test data, fluorescence microscope and transmission electron microscopy images are provided, which yield insight into the antibacterial action of the nanoscale materials. Surprisingly, the results showed graphene oxide (GO) exhibits superior bactericidal effect even at extremely low dose in water (250 μg/mL), almost killing 94.48 % cells, in comparison to common bactericide bismerthiazol with only 13.3 % mortality. The high efficiency in inactivating the bacteria on account of considerable changes in the cell membranes caused by the extremely sharp edges of graphene oxide and generation of reactive oxygen species, which may be the fatal factor for bacterial inactivation. Given the superior antibacterial effect of GO and the fact that GO can be mass-produced with low cost, we expect a new application could be developed as bactericide for controlling plant disease, which may be a matter of great importance for agricultural development.

Keywords *Xanthomonas oryzae pv. oryzae* · Graphene · Antibacterial activity · Mechanisms · Bactericide · Agriculture

Introduction

Xanthomonas oryzae pv. oryzae (*Xoo*), a rod-shaped, Gram-negative species, represent one of the most common pathogens which are the causative agent of bacteria infections causing bacterial leaf blight of rice (*Oryza sativa*) (Ryba-White et al. 1995). Bacterial leaf blight is recognized as one of the most devastating crop bacteria diseases in tropical Asian countries and can cause severe yield loss of up to 50 % in rice (Mew 1987). Protection of crops plant from bacterial disease can substantially improve agricultural production. Commonly, the effective antibacterial agents applied to controlling the plant diseases are confined to synthetic or fumigant chemicals including inorganic bactericide, triazoles, antibiotic, metallic compound biocides (organosulfurs, nitrogen compounds, etc.), which accompany with adverse impact on the environment (Monroc et al. 2006). Moreover, antimicrobial resistance in plant pathogenic target bacteria also brought about the accumulation of the compound, which can result in unimaginably long-term consequences (Imfelda and Vuilleumierb 2012). Another

Electronic supplementary material The online version of this article (doi:10.1007/s11051-013-1658-6) contains supplementary material, which is available to authorized users.

J. Chen · X. Wang · H. Han (✉)
State Key Laboratory of Agricultural Microbiology, College of Science, Huazhong Agricultural University, Wuhan 430070, People's Republic of China
e-mail: hyhan@mail.hzau.edu.cn

approach for preventing the disease is to improve the disease resistance of rice by means of the new transgenic technique, yet it is hard and money-consuming (Gu et al. 2005). Consequently, it is very urgent to develop alternatives to green antibacterial to prevent crop from pathogens infections to avoid the above-mentioned adverse effects (Vidaver 2002).

Recently, carbon nanotubes (CNTs), nanoscale graphene oxide (GO), and reduced graphene oxide (rGO) have been exhibited extremely antibacterial action against major foodborne pathogens like *Escherichia coli* (*E. coli*) and *Staphylococcus aureus* (*S. aureus*) (Kang et al. 2008; Akhavan and Ghaderi 2010; Liu et al. 2009). Among these, Liu et al. (2011) also discovered that GO was more toxic to bacteria than rGO and proved that GO kill approximately 90 % bacteria even at such low concentrations of 80 μg/mL. These studies on different species of microorganisms demonstrate that GO perform a wide target of antibacterial activity. In addition, they are believed to be mild cytotoxicity toward mammalian cells and have also been used for medical disinfection, cellular imaging and drug delivery (Balandin et al. 2008; Bolotin et al. 2008; Jin et al. 2010; Yang et al. 2008). The effectiveness of graphene as antimicrobial agents may be attributed to its extraordinary properties, such as good thermal stability, high surface area, exceptional physiochemical properties, high electronic conductivity, and excellent mechanical strength (Bai and Shen 2012; Hu et al. 2010; Vila et al. 2012). Several studies specifically have proposed that suspensions of sharp GO nanosheets produce either disorganization of cell membrane or oxidative stress which thought to be responsible for high activity of nanoparticles (Akhavan and Ghaderi 2010; Bolotin et al. 2008).

Though graphene and its derivatives were previously shown to be a broad spectrum bactericidal agent active in vitro against both gram-positive and gram-negative pathogenic bacterium (Akhavan and Ghaderi 2010), their action against plant pathogenic bacterium has not been studied. Only recently, one report was put forward that CNTs and GO had superior inactivation effects on copper-resistant *Ralstonia solanacearum* (*R. solanacearum*) and cell membrane damage is the causative factor (Wang et al. 2013). Practically, breakdown of resistance is greatly essential for controlling plant pathogen *Xoo*. Though, biotechnology has been used to overcome the problem but the way is restricted to the genetic engineering of pathogen-resistant plants (Leach et al. 1995). GO has never reported to cause bacterial resistance for complicating bacterial infections therapy. Besides, its germicidal activity and low cost caused by the cheap raw material have much more advantages over traditional bactericides or other chemical compound (Bolotin et al. 2008; Hummers and Offeman 1958; Liu et al. 2008). Thereby, it is indispensable to clarify their cytotoxicity on phytopathogenic bacterium and extend its general function to be potentially applied to design strategies for plant bacterial disease management.

Toward this purpose, a systematic evaluation of graphene oxide and reduced graphene oxide (rGO) against selected plant pathogenic bacterium *Xoo* was investigated for the first time. Specifically, how the material affects cell growth and the mechanisms of contact interaction of graphene with the bacteria are examined. The results found GO could create lethal effects on bacteria, not only due to physically injury the cell structure but also chemically induce harm oxidation action. The unique advantage of physical injury, which current chemical pesticide cannot be beyond the reach of, guarantee this nanoparticle to be efficacious antibacterial agent for eliminating or completely killing surrounding drug- and multidrug-resistant plants infected bacterium. It is anticipated that the research to a certain extent will promote the better application in the biology field and the development of nanoscience and nanotechnology (Hussain et al. 2009).

Methods and materials

Synthesis of GO and rGO

GO was prepared from nature graphite powders by the modified Hummers method (Hummers and Offeman 1958). First, the nature graphite powders (99.99 %; Sigma-Aldrich) were oxidized to produce graphite oxide (GtO). After being washed using deionized water to remove chemical residues, the produced GtO dispersed in deionized water was sonicated (Elamsonic, S60H) for 2 h to exfoliate the GO. The obtained brown GO was reduced to rGO by hydrazine hydrate (Liu et al. 2011), and the reduced graphene oxide was dispersed by bath sonication at 200 W for 2 h. Bismerthiazol (93.7 %) was bought from Hubei provincial seed company.

The two types of materials were characterized by several techniques. The particle stability and size of GO and rGO dispersions were evaluated with dynamic light scattering (DLS) on Malvern Zetasizer Nanoseriesa (Malvern, England). A drop of dispersion was spreaded on a freshly cut mica surface and let the samples air-dried for AFM analysis which obtained on (Agilent 5500) and the ultraviolet absorption spectra were acquired on the Nicolet Evolution 300 UV–Vis spectrometer. The morphology of graphene was inspected and obtained by TEM (Hitachi H-7650, Japan). The Raman spectra were obtained in Via Raman spectrometer (Renishaw, UK) equipped with a confocal microscope (Leica, DM LM/P/11888500, Germany). Fourier transform infrared (FT-IR) spectra were performed on a Nicolet Avatar-330 spectrometer with 2 cm^{-1} resolution using the KBr pellet technique.

Bacterial cell preparations

Xanthomonas oryzae pv. oryzae was purchased from the State Key Laboratory of Agricultural Microbiology of Huazhong Agricultural University. *Xoo* was grown in LB (Luria–Bertani) broth medium in a humidified incubator at 30 °C with constant agitation over night. The bacteria cultures were harvested in the midexponential growth phase and centrifuged at 6,000 rpm for 5 min to collect the cells, and then the bacteria bread was washed three times with deionized water in order to wipe off medium constituents and other chemical macromolecules. After that, cells were resuspended in deionized water, 0.9 % NaCl, and 0.1 M phosphate buffer solution (pH 7.0), and the suspensions were diluted to desired concentration of 10^7–10^8 colony-forming units (CFU/mL), respectively. We will utilize DI water, 0.9 % NaCl and PBS as abbreviations throughout this article. All experiments were carried out at room temperature.

Bacterial cells growth curve

To examine the bacterial growth rate, and the growth curve of bacteria was determined. 200 μL of the diluted cells suspensions mixed with 20 μL of different test concentrations (50, 100, 150, 200, and 250 μg/mL) of GO, rGO, or bismerthiazol was incubated at 30 °C for 2 h with gentle shaking. The control sample contained 200 μL of the cell suspensions added to 20 μL of DI water. The mixture was then transferred to 5 mL tubes containing 2 mL LB medium and the tubes were kept rotating on a shaker at 120 rpm at 30 °C. All treatments were prepared in triplicate. Cells growth was detected by measuring the optical density (OD) at 600 nm every hour on the Nicolet Evolution 300 UV–Vis spectrometer. OD of 0.1 corresponds to a concentration of about 10^8 colony-forming units per ml. Growth curves were created by plotting logarithm of colony-forming units versus time (Dang et al. 2012).

Antibacterial investigations

The antibacterial activity of the graphene-based materials was evaluated by the viability of the bacterial cells with the colony counting methods. 200 μL of cell suspensions (10^7–10^8 CFU/mL) were incubated with 20 μL different test concentrations (50, 100, 150, 200, 250 μg/mL) of GO, rGO, or bismerthiazol for 2 h at 30 °C with gentle shaking, respectively. Then 20 μL serial 10^6-fold diluted with three buffer solutions was spread onto LB plates and left to grow for 2 days at 30 °C. Colonies were counted and calculate the bacterial cell viability compared with control plates method. All treatments were repeated on at least three separate occasions. The cell death rate (% of control) is express as the percentage of (counts of control − counts of treat samples)/counts of control.

Effluxes of DNA and RNA and cell morphology observation

The normal bacteria have integrated membrane. If the cell membrane is disrupted, the vulnerable cell membranes will release some intracellular materials, such as DNA and RNA, and can be monitored at 260 nm by UV absorption (Chen and Cooper 2002). 200 μL portion of different concentration GO or rGO was incubated with 2 mL bacteria suspensions(10^7–10^8 CFU/mL) for 2 h at 30 °C. Then, the mixed suspensions were immediately filtered with 0.22 μm syringe filters to remove the bacteria and the filtrate was examined by the absorbance at 260 nm. Further, the morphology of *Xoo* cells was observed by transmission electron microscopy (TEM) after incubation with GO or rGO. Specifically, after centrifugation at 6,000 rpm, the condensed bacteria were fixed with 2.5 % glutaraldehyde, postfixed with 1 %

aqueous OsO_4 (Fluka) and washed with 0.1 M, pH 7.0 phosphate buffers. Then, samples were dehydrated in an ascending ethanol series (30, 50, 70, 80, 90, and 100 %) for 15 min, respectively, and dried in a vacuum oven. Finally, thin sections containing the cells were placed on the copper grids and were conducted under Tecnai G20 microscopy (FEI, Czech) (Liu et al. 2011).

Fluorescence imaging

The bacterial cell death rates and membrane integrity were further verified by the LIVE/DEAD viability assay (Kang et al. 2008). Briefly, after incubation with 100 μL of GO or rGO (250 μg/mL) at 30 °C for 2 h, the cells were harvested by centrifugation in a microcentrifuge at 6,000 rpm and suspended in 1 mL of water and stained with 10 μL propidium iodide (PI; excitation/emission at 535 nm/617 nm; Sigma-Aldrich) for 15 min and then counter-stained with 10 μL 4′,6-diamidino-2-phenylindole (DAPI, excitation/emission at 358 nm/461 nm; Sigma-Aldrich) for 5 min in the dark, respectively. Then, the samples were observed under inverted fluorescence microscope (Eclipse Ti, Nikon). The cell growth inhibition percentage was from the ratio of the number of cells stained with PI (dead bacteria) divided by the number of cells stained with DAPI plus PI (total bacteria).

Detection of reactive oxygen species

The reactive oxygen species (ROS) production in the bacterial growth medium were investigated using the oxidation sensitive fluorescent dye 2′,7′-dichlorofluorescin diacetate (DCFH-DA, Sigma-Aldrich), which is a kind of ROS-detecting agent (Tan et al. 2009). DCFH-DA is a nonfluorescent compound, after it enters the cell, it was commonly hydrolyzed to 2′,7′-dichlorofluorescin (DCFH-DA) by esterase and oxidized to DCF due to the presence of ROS. The increasing fluorescence intensity of DCF indicates the level of intracellular ROS. In brief, 300 μL of GO or rGO dispersions (the control with DI water) were incubated with 3 mL bacteria suspensions for 2 h at 30 °C, the bacteria then were washed three time with 0.1 M PBS (pH 7.8) solution and resuspended in 3 mL 0.1 M PBS (pH 7.8) solution. A drop of DCFH-DA with a final concentration of 10 μM was added to the bacteria suspensions and incubated in the dark for 1 h. The mixture immediately was washed to remove the DCFH-DA without oxidation. The fluorescence generated by the DCF oxidation was measured on an Edinburgh FLS920 spectrometer at 522 nm. The level of intracellular ROS was expressed as a percentage of control cells.

Measurements of thiols contents

In this experiment, the loss of thiol groups (–SH) on the proteins was quantified by a Thiol and Sulfide Quantization Kit (Molecular Probes, Abigen) used in previous study (Liu et al. 2011). 200 μL of GO or rGO dispersions at 250 μg/mL in DI water were incubated with 0.5 mL of *Xoo* (10^7–10^8 CFU/mL) suspensions for 2 h at 30 °C. The bacteria then were centrifuged at 6,000 rpm for 10 min and washed three times in DI water. After being resuspended in water, the cells were lysed by sonication at 200 W for 1 min. The supernatants were used for assay. The protein concentrations in cell extracts were determined by a Pierce BCA protein assay kit. The assays were performed to assess the GO and rGO oxidation of proteins according to the manufacturer's protocol of the kit.

Statistical analysis

Data are expressed as mean and standard deviations of a representative of three experiments carried out in triplicate. Error bars represent the standard deviation of the mean. The significant difference of data was analyzed using the Statistical Package for the Social Sciences (SPSS) version 19.0 software. Statistical comparisons were performed by analysis of variances (ANOVA). The value of p (<0.05 and <0.01) which were denoted * and **, defined as significant difference.

Results and discussion

Characterization of GO and rGO dispersions

We prepared the GO and rGO dispersions using the methods described in "Methods and materials" section. As shown in Fig. 1, we displayed the visual photos and the dynamic light scattering size distribution of the graphene solution, showing that the average

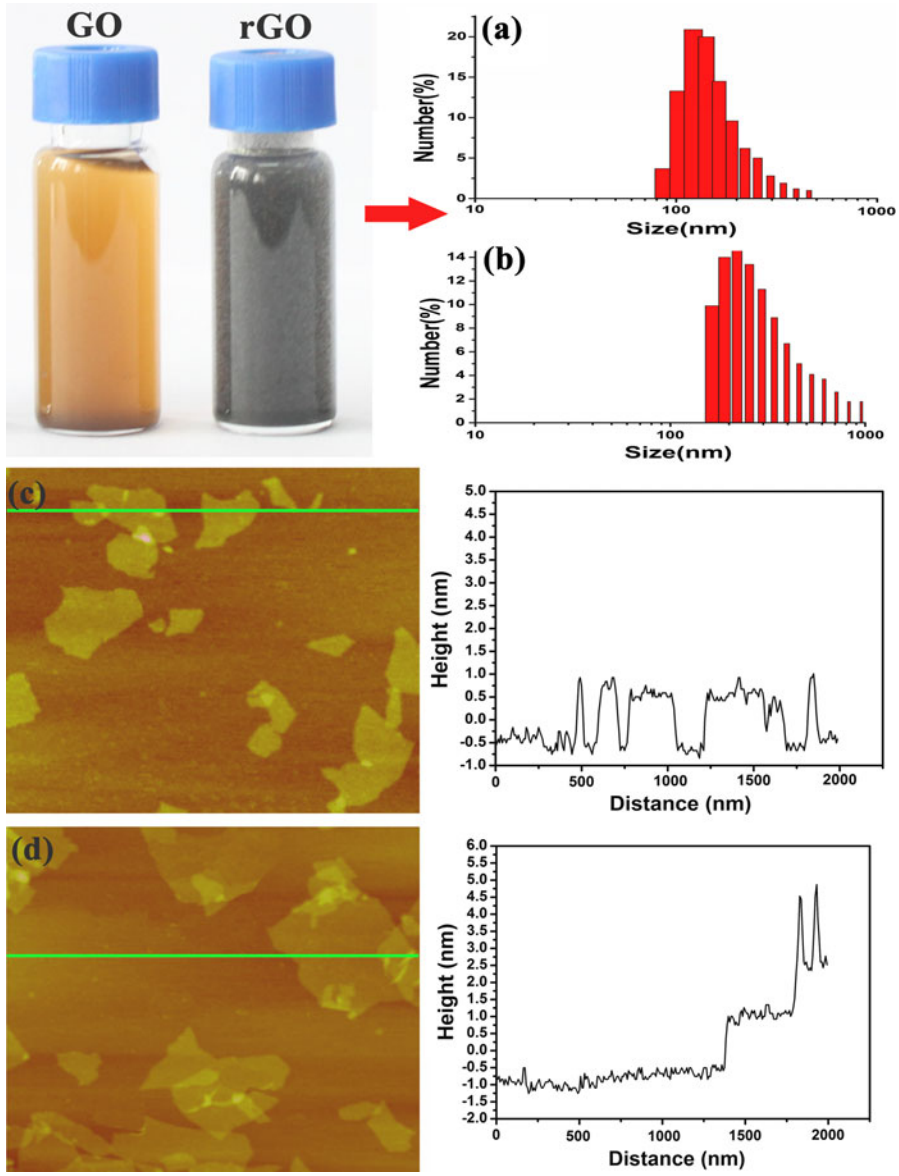

Fig. 1 Visual image of GO and rGO water dispersions and size distribution of GO (**a**) and rGO (**b**) in water using dynamic light scattering after 2 h sonication. AFM height image of exfoliated GO (**c**) and rGO (**d**) nanosheets dried on amica surface and the corresponding height profile of the AFM image

size of the nanosheets was between 300 and 600 nm. The size of rGO is much larger than that of GO because of the aggregation of rGO fragments. It is observed that GO presented clear and yellow-brown dispersions but black and turbid for rGO dispersions. The differences between them derive from some hydrophilic functional groups on the surface of GO nanosheets (Stankovich et al. 2007). AFM measurements revealed that exfoliated GO were flat sheets with an average thickness of 0.76 nm. rGO presented disorganized aggregation and had a reduced sheet thickness of 1.59 nm (Fig. 1c, d), which was possibly attributed to partial removal of oxygen functional groups on the surface of GO nanosheets during the reduction process.

TEM image revealed that GO sheets had smooth with small wrinkles at the edges, while rGO thin sheets became randomly folded and aggregated. The crumpled sheets closely associate with each other and forming a disordered solid (Fig. 2b). As shown in Fig. 2c, the Raman spectrum of GO contains high intensive G and D bands at 1,590 and 1,350 cm^{-1}, due to the extensive oxidation. rGO displays G and D peaks at 1,586 and 1,329 cm^{-1}. However, an

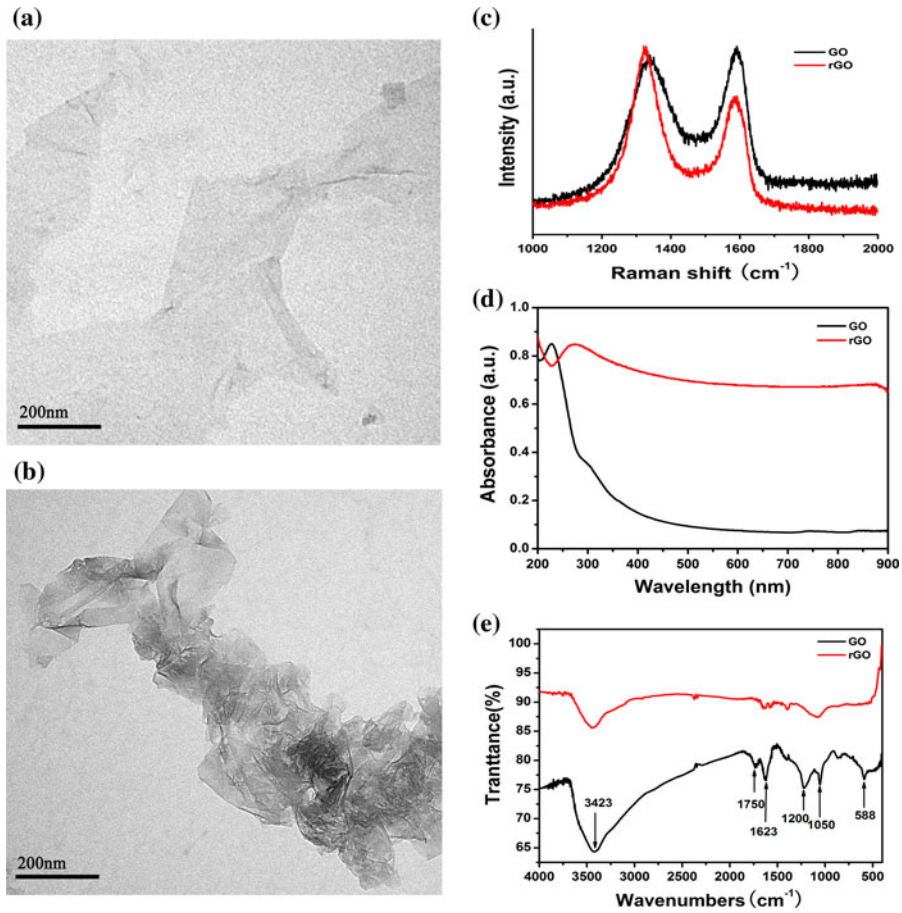

Fig. 2 TEM images of graphene oxide nanosheets (**a**) and aggregated reduced GO sheets (**b**). **c** Raman spectra of GO and the rGO. **d** UV–Vis absorption spectra and **e** FT-IR spectrum of GO and rGO

increased D/G intensity ratio of rGO compared to that of the GO is observed, indicating a decrease in the average size of the sp^2 domains upon the reduction of the GO and the GO has been well deoxygenated in rGO (Xu et al. 2008). The UV–Vis absorption peak of GO is 230 nm involving π–π* transitions of aromatic C=C bonds which is gradually red-shifted to 267 nm in comparison with that of rGO. It is indicated the π-conjugation network restore within the G nanosheets (Zhou et al. 2009) (Fig. 2d). FT-IR spectrum of GO and rGO in Fig. 2e demonstrated the fully oxidation of graphite and reduced by hydrazine hydrate, which successfully formed GO and rGO, respectively. GO vibrated characteristically at the broad and intense peak of –OH group at 3,423 cm^{-1}, strong C=O peak at 1,750 cm^{-1}, the C–OH stretching peak at 1,200 cm^{-1}, and the C–O stretching peak at 1,050 cm^{-1}. After reduced using hydrazine, the adsorption bands of oxygen functionalities (such as carboxyl groups, C–OH) weakened or almost disappeared. Only two broad peaks at 3,400 and 1,047 cm^{-1} were found for rGO in Fig. 2e, which could be assigned to the –OH group of remaining water and C–O stretch, respectively (Xu et al. 2008). On the other hand, the strong van der Waal makes the rGO particles aggregated, inducing bad dispersibility. These examinations confirmed that GO and rGO were well synthesized.

Inhibition of bacterial growth after treatment with GO and rGO dispersions

The growth inhibitory effect of GO and rGO in different buffers against plant pathogenic bacteria *Xoo* was initially evaluated by means of measuring the growth curves of the bacteria during the 8-h cultivation.

Figures 3 and 4 represent the growth inhibition assays for *Xoo*. The bacterial growth was observed during the first 8 growth hours (lag phase and exponential phase). The results showed that GO and rGO caused a growth delay of *Xoo*, primarily depending

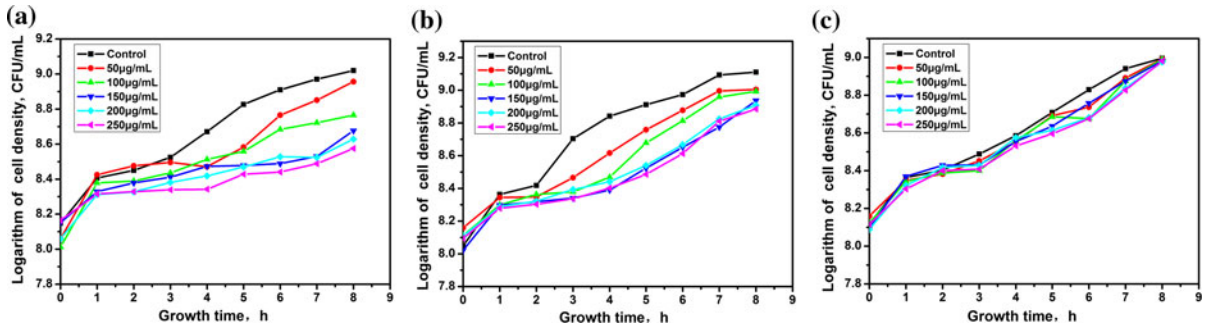

Fig. 3 Growth curves of *Xoo* after treatment with various concentrations of GO in different buffers for 2 h: **a** in DI water, **b** in 0.9 % NaCl, and **c** in pH 7.0, 0.1 M PBS. All concentrations referred to the final concentration in the treatment solutions. The control cells were being treated with DI water

on the concentration and the type of buffer. At a given point of growth, it was important to note that the bacteria growth rate significantly decreased with increasing concentration of GO in DI water and 0.9 % NaCl, yet a little decrease in 0.1 M PBS. A dose-dependent elongation in the time reach the exponential phase was demonstrated in *Xoo* cells exposure to GO. Obviously, compared with the control which required approximately 2.2 h, the growth time of the cells treated with 50, 100, 150, 200, and 250 μg/mL of GO dispersions in DI water were 3.0, 3.5, 4.0, 5.0, 6.8 h or so, delayed by approximately 5 h at the highest concentration of 250 μg/mL (Fig. 3a). Similarly, Fig. 3b showed that the cells treated with GO in 0.9 % NaCl delayed exponential growth for approximately 0.5, 1.3, 1.6, 2.0, and 2.2 h, respectively. The shorter time to reach the exponential phase required, the more vigorous the cells are. It means that there were few surviving cells in the mixture after treatment with GO dispersions in both buffers compared with the control sample, indicating stronger antibacterial activity. Differently, it was shown in Fig. 4a, b, growth of *Xoo* tested in rGO dispersions in DI water and 0.9 % NaCl with varying concentrations was weakly affected.

As seen from the growth inhibition rates in Figs. 3 and 4, GO and rGO showed the better inhibitory effect in DI water than in 0.9 % NaCl and the antibacterial activities greatly depended on the buffer solutions in our experiment. Moreover, it should be noted that GO exhibited much stronger antimicrobial activity in DI water and 0.9 % NaCl than rGO from the growth curves. However, there was nearly no significant difference in the time reached to the exponential phase between the groups in 0.1 M PBS, which showed no obvious bacterial growth inhibition. The results can be attributed to the effects of the ionic strength on the interactions between the bacterial cell and the CNMs (Liao et al. 2011). However, the growth of bacteria was not affected by the exposure to bismerthiazol (Fig. S2a in supplementary material).

Bactericidal effect of GO and rGO dispersions toward *Xoo* cells

Previous studies showed carbon nanomaterial have strong antibacterial activity and the antibacterial activities of CNTs and GO depended on the size, aggregate state, buffer type, and concentrations (Moore et al. 2003; Kang et al. 2008; Dong et al. 2008; Liao et al. 2011). The colony-forming units method (CFU) was used to further verify the mortality of *Xoo* cells in different solutions from the growing cells in the presence of different concentrations of GO and rGO dispersions. *Xoo* cell suspensions dispersed in DI water, 0.9 % NaCl, and 0.1 M PBS (10^7–10^8 CFU/mL) mixed with the nanomaterials at the same shaking speed (120 rpm) for 2 h, respectively. The samples without graphene were used as a control. It well also shows buffer and dose-dependent antibacterial activity of GO and rGO dispersions. We demonstrate that the concentration range of 50–250 μg/mL suspensions of GO could effectively inhibit the microorganisms. As presented in Fig. 5, the bacteria death rate significantly soared in order of concentration of GO and rGO dispersions. GO exhibited much stronger antibacterial activity in both DI water and 0.9 % NaCl with the cell mortality 94.48 and 86.4 % at 250 μg/mL compared with 36.11 and 22.31 % of cell death with rGO treatment, respectively. Whereas bismerthiazol only killed 13.3 % of

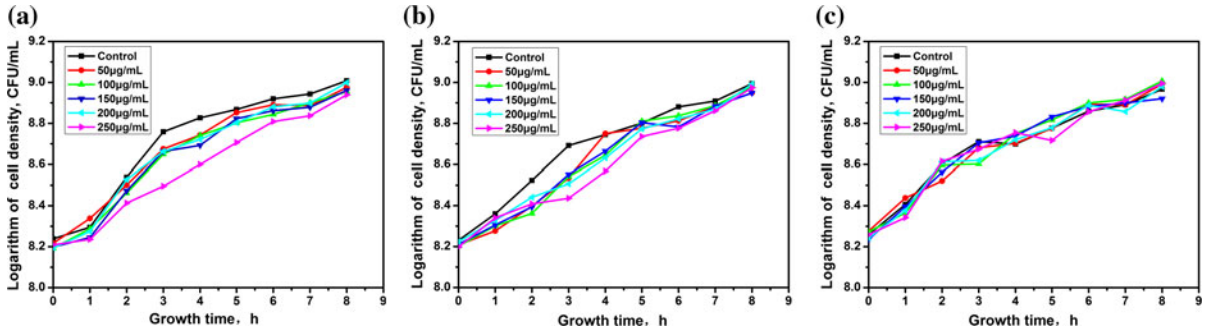

Fig. 4 Growth curves of *Xoo* after treatment with various concentrations of rGO in different buffers for 2 h: **a** in DI water, **b** in 0.9 % NaCl, and **c** in pH 7.0, 0.1 M PBS. All concentrations referred to the final concentration in the treatment solutions. Control cells were being treated with DI water

bacteria at 250 μg/mL in DI water (Fig. 6c). These results confirm GO has higher antibacterial activity than rGO, which displays the same effect as previous reports (Liu et al. 2011; Hu et al. 2010). The LB-agar plate images exhibited the bacterial colony after treatment with different concentrations of GO and bismerthiazol (Fig. S1a in supplementary material). This phenomenon can also support our results that GO has not only bacteriostatic activity but also bactericidal effect toward *Xoo* in DI water. Nonetheless, it is interesting that both GO and rGO present stronger antibacterial activity in DI water than in 0.9 % NaCl and they present scarcely any bacteriostatic activity in 0.1 M PBS even at the highest concentration of 250 μg/mL, inducing few bacteria cells loss. These findings were consistent with the rate of the growth inhibition from the bacteria growth OD curve.

As control experimental results, all three solutions are suitable for bacteria growth in which cells show very similar vigor having the same growth curve and survival rate as illustrated in Fig. 3 and Figure S1 in supplementary material. Therefore, the remarkably different antibacterial activities presented in Fig. 5 can be attributed to the distinct GO interaction action with bacteria in different dispersant. It was reported that GO was soluble and possessed well dispersity stationarity in water but aggregated in solutions with rich salts (Liu et al. 2008). The iron strength in the salts may affect the interaction between bacteria and nanomaterial (Liao et al. 2011). The properties make clear that GO sheets have strongest antibacterial activity in water and significantly inhibit the cell growth (Fig. 3).

We also investigated the effect of incubation time on the inhibitory activity of the nanoparticles in DI water (Fig. 6). The representative concentrations of the lowest (50 μg/mL) and highest (250 μg/mL) were used. The cells were incubated with GO or rGO solutions for 1–4 h at 30 °C, respectively. These results also show that incubation time is an important factor when graphene put into effect antibacterial activities on *Xoo*.

As observed in Fig. 6a, the cell mortality rate was obviously greater than the control and the death became more serious with increasing incubation time at both concentrations. The cell death percentage ascended from 19.43 to 66.09 % at 50 μg/mL and from 47.78 to 88.6 % at 250 μg/mL after incubation with GO dispersions extending from 1 to 4 h. And the loss of cell viability increases from 10.82 to 24.77 and 13.85 to 30.53 % for the rGO dispersions, respectively (Fig. 6b). Results in these study found that the antibacterial activity of GO toward plant pathogen is also largely determined by factors of concentration, buffer type, and time.

Furthermore, since the high antibacterial activity of GO is observed in the present study, the effect of the nanomaterials on the plant should be taken into a major consideration for future application. It was found previously that the graphene materials increased growth rates of tomato in the seedling stage at 50 μg/mL, with no sign of significant toxicity. Little toxicity of GO for some kinds of plants was also investigated at concentrations of 500–2,000 μg/mL (Khodakovskaya et al. 2011; Begum et al. 2011). Thus, it can be believed that GO could strongly inactivate *Xoo* at such low concentration (50–250 μg/mL) in our experimental conditions, which may have little influence on crop.

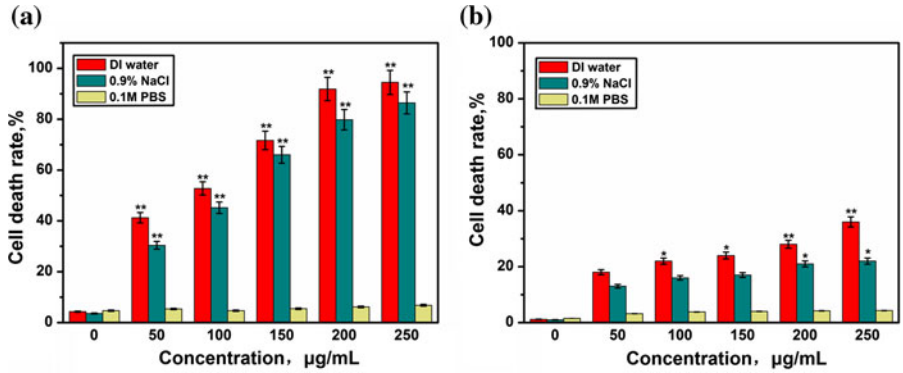

Fig. 5 Cell death rate after incubation with GO (**a**) and rGO (**b**) dispersions at different concentrations (0–250 μg/mL) in different buffers for 2 h at 30 °C. *Xoo* suspension without graphene-based materials was used as control. Error bars represent the standard deviation. $*p < 0.05$ and $**p < 0.01$

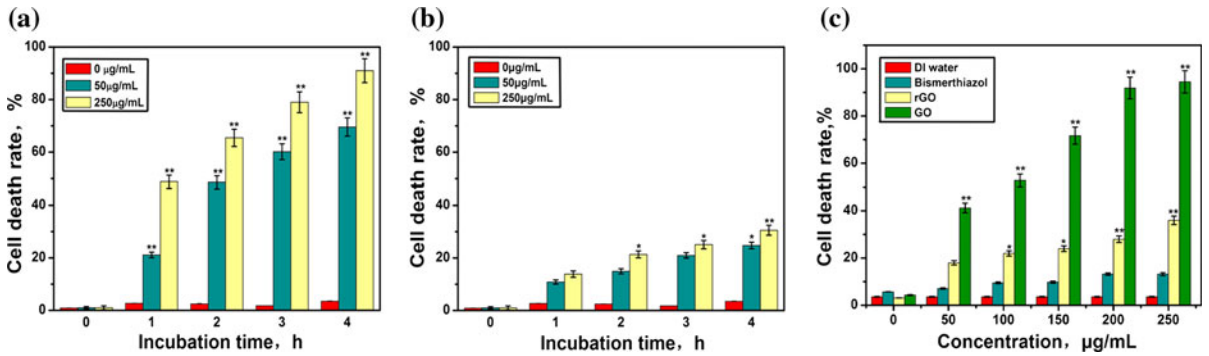

Fig. 6 The effects of incubation time on the cell mortality after treatment with GO (**a**) and rGO (**b**) dispersions in DI water. GO or rGO (20 μL) was incubated with *Xoo* (10^7–10^8 CFU/mL, 200 μL) in DI water for 4 h at 30 °C. The data was measured at intervals of 1 h. **c** Cell death rate after incubation with bismerthiazol, GO, and rGO dispersions at different concentrations (0–250 μg/mL) in DI water for 2 h at 30 °C. *Xoo* suspension without graphene-based materials was used as control. *Error bars* represent the standard deviation. $*p < 0.05$ and $**p < 0.01$

Study of antibacterial mechanisms of graphene

Destruction of bacterial membrane

From the results above, it can be concluded that GO solution dispersed in DI water has stronger bactericidal effect at both concentrations than rGO dispersions. Therefore, the following mechanism investigation of this study will focus on the *Xoo* incubated with GO in DI water.

To verify the reliability of the CFU method in the study, *Xoo* is used to further examine the death rates after incubation with graphene dispersions by fluorescence dye methods. After treatment with GO and rGO at 250 μg/mL, the bacteria suspensions in water were dyed using fluorescence agent (DAPI and PI) according to previous studies (Kang et al. 2008). DAPI can pass through an intact cell membrane and bind strongly to DNA which stains live cells with blue fluorescence. PI is membrane impermeable which commonly stains dead cells with red fluorescence. Figure 7 presents the fluorescence microscopy images of *Xoo* suspensions in DI water interacted with GO, rGO, and the control (i.e., without any materials). Visually, the untreated cells showed blue fluorescence due to the intact cell wall structure of the viable or live cells in Fig. 7a. In contrast, almost 100 % of bacteria cells treated with 250 μg/mL GO showed red fluorescence indicating dead cells with permeable cell membrane structure (Fig. 7b). However, a majority of cells were live (blue) in rGO dispersions. The results from the studies above are in agreement with cell viability test.

Then, an intriguing conclusion arises from our antibacterial activity results. That is GO dispersions

have higher antibacterial activity than rGO dispersions. Therefore, it is essential to understand how the nanomaterials interact with bacterial cells. Several previous studies have proposed that the antibacterial activity of GO is associated with the damage of cell membrane upon the direct contact between GO and bacteria by Liu et al. (2011) and Akhavan and Ghaderi (2010). From our subsequent studies by TEM in Fig. 8, it can be observed that the thin nanosheets of GO and the large aggregation of rGO fragments. The cell morphology images implied that bacteria cells were wrapped by thin layers of GO sheets after 2 h of incubation. The cells exposed to GO were partly hollow and membranes were probably fractured with some endoplasm outflowing. However, the rGO sheets were just near the bacteria cell and without impinging on them (Fig. 8c). The observed images of cell in this experiment were in similar with previous scanning electron microscope images (Liu et al. 2011; Hu et al. 2010). The better dispersibility and smaller size of GO may correlate to different behavior from rGO.

The UV absorption assay in the particular study was further carried out to verify whether the cell membrane was disorganized when it was exposed to GO and rGO dispersions by measuring the efflux of cytoplasmic materials. If the bacterial membrane is compromised, the release of cytoplasmic constituents, such as DNA and RNA can be monitored by their strong UV absorption at 260 nm. A statistically significant UV absorption at 260 nm was observed in Fig. 9 after incubation with different concentrations of GO dispersions compared with the cytoplasmic constituents concentration of the control sample, but nearly little increase in rGO dispersions. These investigations are in agreement with cell viability measurement. The results from the absorption study confirmed that the DNA and RNA were largely leaked, suggesting that severely injured bacteria cell membrane correlates to the bacterial mortality.

Hence, it can be proposed that smaller, sharper GO sheets can easily wrap and cover the cell surface, affecting metabolic activity such as blocking transport through cell membrane (Liu et al. 2012). Meanwhile, GO sheets interact with cell and damage vulnerable cell membrane, causing cell death. This proposed mechanism may be play the vital role in inactivating the bacterial *Xoo* for GO. The findings mentioned above were similar with our group previous report that graphene oxide showed distinct antibacterial properties against the copper-resistant plant pathogenic bacteria *R. solanacearum* duing to sharp-knife-like GO had more chances to contact bacteria than rGO, thus causing severe damage to cell membrane (Wang et al. 2013). Most of plant pathogens are gram-negative bacterium, having the similar structure to *Xoo*. Thus, it is presumable that the high performance of graphene maybe open up new possibilities for inactivating on multi-plant pathogenic microorganisms.

Production of intracellular oxidative stress

Finding in the experiment, the observation of GO attached to the cell membrane and physically injure them is fundamental to understand the bactericidal

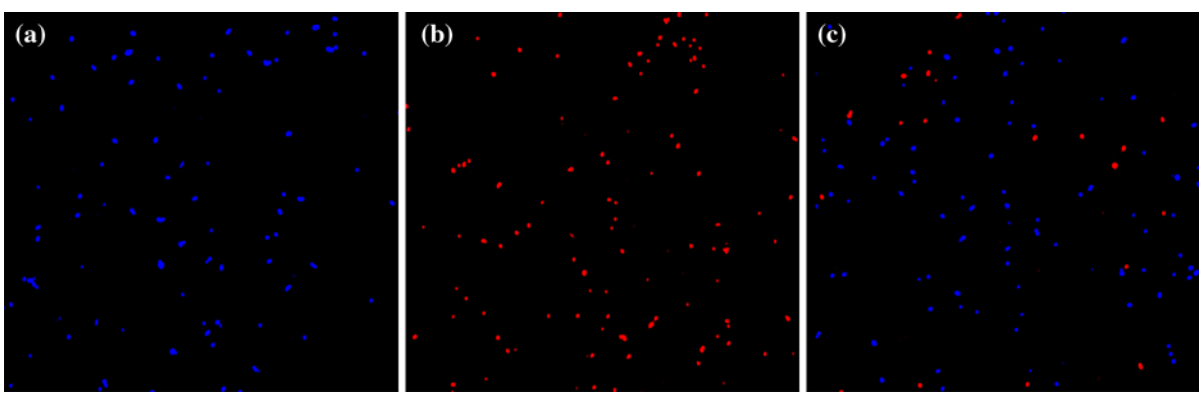

Fig. 7 Fluorescence microscope image of *Xoo* total cells in DI water (cells stained with propidium iodide and DAPI) after incubation with GO (**b**) and rGO (**c**) dispersions at the concentration of 250 μg/mL, the cells treated with water as control (**a**). The cells were observed directly at 100× magnification by fluorescence microscopy. *Red* stands for dead cells and blue stands for live cells

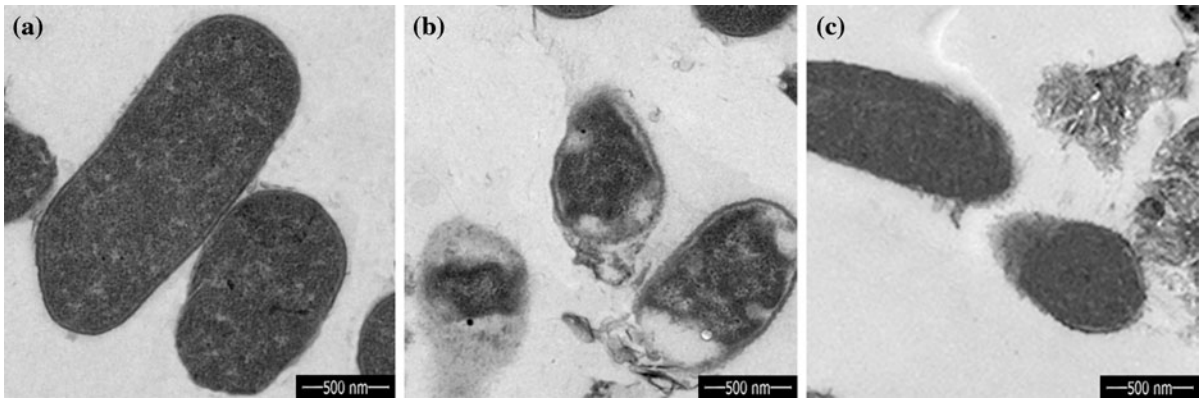

Fig. 8 TEM images of *Xoo* cells treated without nanomaterials (**a**), with GO (**b**), and rGO (**c**) suspensions. 100 μL of GO and rGO dispersions (250 μg/mL) were incubated with 1 mL bacterial suspensions (10^7–10^8 CFU/mL) for 2 h at 30 °C

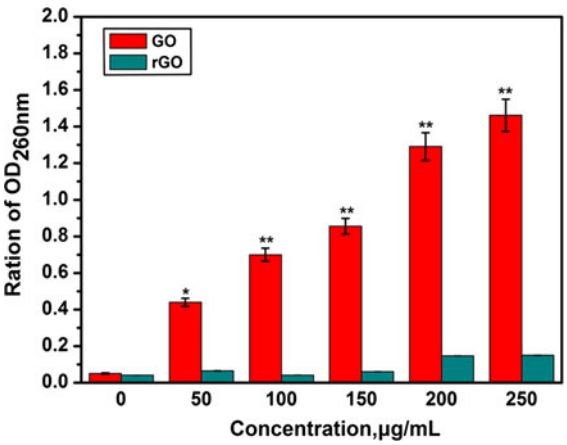

Fig. 9 The absorbance of efflux of cytoplasmic materials (DNA and RNA) at 260 nm after cells being incubated with different concentrations of GO and rGO, respectively. 200 μL of GO and rGO dispersions were incubated with 2 mL bacterial suspensions in DI water (10^7–10^8 CFU/mL) for 2 h at 120 rpm shaking speed, and 30 °C. Error bars represent the standard deviation. $*p < 0.05$ and $**p < 0.01$

mechanism. Also, except for the physical membrane damage, the toxicity of graphene largely due to oxidative stress toward neural cells (Zhang et al. 2010). Thiol groups of glutathione (GSH) as an antioxidant in protein can be oxidized to disulfide bond, forming defense mechanisms in the cellular against oxidative stress (Liu et al. 2011). So, the consume content of GSH can reflect the ability of cells against oxidative stress. We assessed the level of thiols groups in cellular protein after the bacteria were incubated with GO and rGO dispersions using a Thiol and Sulfide Quantization Kit. As shown in Fig. 10a, after bacteria exposure to both of the dispersions, the loss of GSH significantly increased with the gradual increase of concentration compared with the control, which demonstrated the GO and rGO can induce oxidation of GSH and the dose-dependent effects was consist with the foregoing results. Some previous studies demonstrated that oxidative stress played an important role in the antibacterial mechanism of CNT (Arias and Yang 2009; Liu et al. 2009) and C_{60} (Lyon and Alvarez 2008; Hotze et al. 2008). It was proved that rGO possessed higher oxidative capacity than GO. The difference may attribute to the much higher conductivity of rGO. Graphene oxide is electrically insulating materials because of their disrupted sp^2 bonding networks. When GO is reduced to rGO, the π network will be restored and the electrical conductivity can be recovered (Zhou et al. 2009). Therefore, rGO can oxidize more GSH than insulating GO, which suggested the chemistry properties of the materials determine its antibacterial actions.

Another oxidative damage to cells is the production of ROS. To detect the accumulation of ROS, *Xoo* bacteria cells were exposed to GO at various concentrations. The ROS content was measured using the fluorescence intensity of the fluorescent ROS-indicator DCFH-DA. In the presence of GO dispersions, the ROS production significantly increased in a concentration-dependent manner compared with the control group, even at the lowest concentration (50 μg/mL). The fluorescence intensity was nearly 5-fold of control after exposure to the highest concentration of 250 μg/mL. A small amount accumulation of ROS content also displayed in Fig. 10b when the bacteria cells

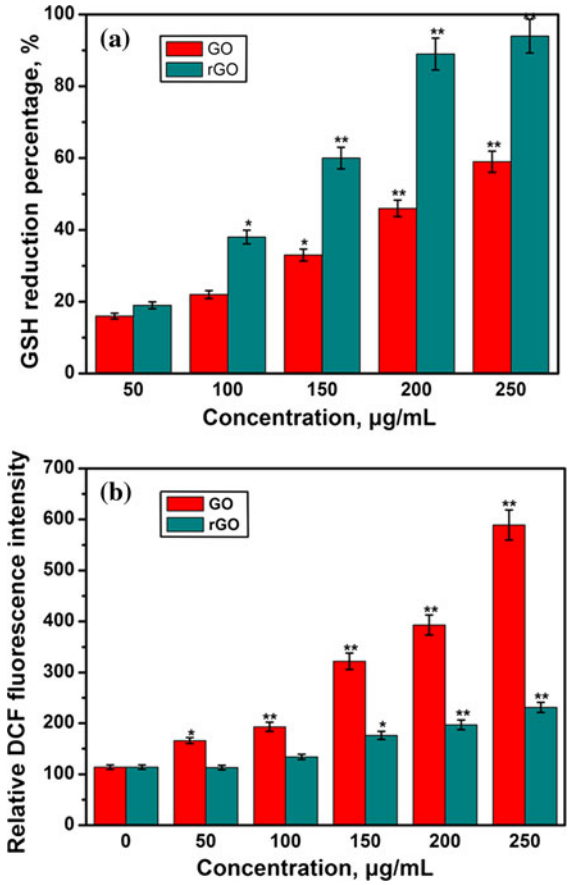

Fig. 10 **a** Thiol oxidation and **b** ROS generation after the bacteria suspensions in DI water incubation with graphene oxide and reduced graphene oxide dispersions at various concentrations for 2 h. The sample without materials was used as the control. *Error bars* represent the standard deviation. $*p < 0.05$ and $**p < 0.01$

treating with rGO dispersions, which was only 2-fold of the control at the higher concentrations. It has been reported that GO-induced superoxide anion-independent oxidation and ROS production toward bacteria and cells (Liu et al. 2011). GO mediated higher level ROS production than rGO, probably due to their different physicochemical properties, such as size, conductivity, and functional group in the surface. Meanwhile, we did the cell-free assay and the result showed there was no fluorescence generation when GO and rGO only incubated with DCFH-DA (Fig. S3 in supplementary material), which suggest that the nanomaterials would not direct oxidize the fluorescence dye. The finding is in agreement with the previous conclusion that there was no signal with the XTT assay (Liu et al. 2011). It was concluded that the DCF fluorescence was obtained through the intermediary of ROS production in bacteria rather than directly oxidized by nanoparticles. Namely, GO can led to oxidative stress toward the bacteria *Xoo* by inducing the generation of ROS.

Conclusion

In conclusion, we discussed the antibacterial action of GO toward the phytopathogenic bacterium *Xoo* for the first time. The results of this study have demonstrated that GO had the extremely prominent dose-dependent inhibitory effect on cell growth utilizing growth inhibition assay and colony-forming count method. The mechanism may be the combination of direct membrane damage and oxidative stress, possibly acting synergistically. With the application potential, the advantages of inhibiting or killing bacteria by graphene oxide presumably include three respects compared to other antibacterial materials or agents. First, the antibacterial mechanism of GO caused by both mechanically physical injury and chemical oxidation which is hard to cause bacterial resistance. Second, GO is environment-friendly and presents mild cytotoxicity to mammalian cells and some plant within such low dose. Third, compared to other carbon nanomaterials, the easy processing, large scale production, and inexpensive cost all guarantee it can be a good choice as an antibacterial agent.

Further investigations will be required to understand the molecular basis of graphene oxide action, such as some important response genes expression of bacteria involved in oxidative stress response, pathogenesis and toxin production, making comprehensive understanding the interaction mechanism between the nanoparticles and the pathogen. Our studies would stimulate more toxicology evaluations of graphene and its derivatives. Thus, this powerful new pattern holds great promise as bactericide for multiple pathogenic microorganisms, implying an equipment for crop protection.

Acknowledgments The authors gratefully acknowledge the financial support for this research from National Natural Science Foundation of China (21175051), the Fundamental Research Funds for the Central Universities (2011PY139), and the Natural Science Foundation of Hubei Province Innovation Team (2011CDA115).

References

Akhavan O, Ghaderi E (2010) Toxicity of graphene and graphene oxide nanowalls against bacteria. ACS Nano 4:5731–5736

Arias LR, Yang LJ (2009) Inactivation of bacterial pathogens by carbon nanotubes in suspensions. Langmuir 25:3003–3012

Bai S, Shen XP (2012) Graphene-inorganic nanocomposites. RSC Adv 2:64–98

Baker B, Zambryski P, Staskawicz B, Dinesh-Kumar SP (1997) Signaling in plant-microbe interactions. Science 276:726–733

Balandin AA, Ghosh S, Bao WZ, Calizo I, Teweldebrhan D, Miao F, Lau CN (2008) Superior thermal conductivity of single-layer graphene. Nano Lett 8:902–907

Begum P, Ikhtiari R et al (2011) Graphene phytotoxicity in the seedling stage of cabbage, tomato, red spinach, and lettuce. Carbon 49:3907–3919

Bolotin KI, Sikes KJ, Jiang Z, Klima M, Fudenberg G, Hone J, Kim P, Stormer HL (2008) Ultrahigh electron mobility in suspended graphene. Solid State Commun 146:351–355

Chang YL, Yang ST, Liu JH, Dong E, Wang Y, Cao A, Liu YF, Wang HF (2011) In vitro toxicity evaluation of graphene oxide on A549 cells. Toxicol Lett 3:201–210

Chen CZS, Cooper SL (2002) Interactions between dendrimer biocides and bacterial membranes. Biomaterials 23:3359–3368

Dang TC, Fujii M, Rose AL, Bligh M, Waitea TD (2012) Characteristics of the freshwater cyanobacterium microcystis aeruginosa grown in iron-limited continuous culture. Appl Environ Microbiol 78:1574–1583

Dong L, Joseph KL, Witkowski CM, Craig MM (2008) Cytotoxicity of single-walled carbon nanotubes suspended in various surfactants. Nanotechnology 19(25):255702. doi: 10.1088/0957-4484/19/25/255702

Gu K et al (2005) R gene expression induced by a type-III effector triggers disease resistance in rice. Nature 435:1122–1125

Hotze EM, Labille J, Alvarez P, Wiesner MR (2008) Mechanisms of photochemistry and reactive oxygen production by fullerene suspensions in water. Environ Sci Technol 42:4175–4180

Hu WB, Peng C, Luo WJ, Lv M, Li XM, Li D, Huang Q, Fan CH (2010) Graphene-based antibacterial paper. ACS Nano 4:4317–4323

Hummers WS, Offeman RE (1958) Preparation of graphitic oxide. J Am Chem Soc 80:1339

Hussain SM, Braydich-Stolle LK, Schrand AM, Murdock RC, Yu KO, Mattie DM, Schlager JJ, Terrones M (2009) Toxicity evaluation for safe use of nanomaterials: recent achievements and technical challenges. Adv Mater 21:1549–1559

Imfelda G, Vuilleumierb S (2012) Measuring the effects of pesticides on bacterial communities in soil: a critical review. Eur J Soil Biol 49:22–30

Jin Z, Nackashi D, Lu W, Kittrell C, Tour JM (2010) Decoration, migration, and aggregation of palladium nanoparticles on graphene sheets. Chem Mater 22:5695–5699

Kang S, Herzberg M, Rodrigues DF, Elimelech M (2008) Antibacterial effects of carbon nanotubes: size does matter! Langmuir 24:6409–6413

Khodakovskaya MV, de Silvaa K, Nedosekinb DA, Dervishic E, Birisa AS, Shashkovb EV et al (2011) Complex genetic, photothermal, and photoacoustic analysis of nanoparticle-plant interactions. Proc Natl Acad Sci USA 108:1028–1033

Leach JE, Leung H, Nelson HL, Mew TW (1995) Population biology of *Xanthomonas oryzae pv. oryzae* and approaches to its control. Curr Opin Biotechnol 6:298–304

Liao HH, Qi RL, Shen MW, Cao XY, Guo R, Zhang YZ, Shi XY (2011) Improved cellular response on multiwalled carbon nanotube-incorporated electrospun polyvinyl alcohol/chitosan nanofibrous scaffolds. Colloids Surf. B: Biointerfaces 84:528–535

Liu Z, Robinson JT, Sun XM, Dai HG (2008) PEGylated nanographene oxide for delivery of water-insoluble cancer drugs. J Am Chem Soc 130:10876–10877

Liu SB, Wei L, Hao L, Fang N, Chang MW, Xu R, Yang YH, Chen Y (2009) Sharper and faster "nano darts" kill more bacteria: a study of antibacterial activity of individually dispersed pristine single-walled carbon nanotube. ACS Nano 3:3891–3902

Liu SB, Zeng TH, Hofmann M, Burcombe E, Wei J, Jiang RR, Kong J, Chen Y (2011) Antibacterial activity of graphite, graphite oxide, graphene oxide, and reduced graphene oxide: membrane and oxidative stress. ACS Nano 5:6971–6980

Liu SB, Hu M, Zeng TH, Wu R, Jiang RR, Wei J, Wang L, Kong J, Chen Y (2012) Lateral dimension dependent antibacterial activity of graphene oxide sheets. Langmuir 28:12364–12372

Lyon DY, Alvarez PJJ (2008) Fullerene water suspension (nC_{60}) exerts antibacterial effects via ROS-independent protein oxidation. Environ Sci Technol 42:8127–8132

Mew TW (1987) Current status and future prospects of research on bacterial blight of rice. Ann. Rev. Phytopathol 25:359–382

Monroc S, Badosa E, Besalú E, Planas M, Bardajía E, Montesinosb E, Feliua L (2006) Improvement of cyclic decapeptides against plant pathogenic bacteria using a combinatorial chemistry approach. Peptides 27:2575–2584

Moore VC, Strano MS, Haroz EH, Hauge RH, Smalley RE (2003) Individually suspended single-walled carbon nanotubes in various surfactants. Nano Lett 3:1379–1382

Ryba-White M, Notteghem JL, Leach JE (1995) Comparison of *Xanthomonas oryzae pv.* strains from Africa, north America and Asia by RFLP analysis. Intl Rice Res Notes 20:25–26

Stankovich S, Dikin DA, Piner RD, Kohlhaas KA, Kleinhammmes A, Jia Y, Wu Y, Nguyen ST, Ruoff RS (2007) Synthesis of graphene-based nanosheets via chemical reduction of exfoliated graphite oxide. Carbon 45:1558–1563

Tan XM, Lin C, Fugetsu B (2009) Studies on toxicity of multi-walled carbon nanotubes on suspension rice cells. Carbon 47:3479–3487

Vidaver AK (2002) Uses of antimicrobials in plant agriculture. Clin Infect Dis 34:107–110

Vila M et al (2012) Cell uptake survey of pegylated nanographene oxide. Nanotechnology 13(46):465103. doi: 10.1088/0957-4484/23/46/465103

Wang XP, Liu XQ, Han HY (2013) Evaluation of antibacterial effects of carbon nanomaterials against copper-resistant

Ralstonia solanacearum. Colliods Surf. B Biointerfaces 103:136–142

Xu YX, Bai H, Lu GW, Li C, Shi GQ (2008) Flexible graphene films via the filtration of water-soluble noncovalent functionalized graphene sheets. J Am Chem Soc 130:5856–5857

Yang XY, Zhang XY, Liu ZF, Ma YF, Huang Y, Chen YS (2008) High-efficiency loading and controlled release of doxorubicin hydrochloride on graphene oxide. J Phys Chem C 112:17554–17558

Zhang YB, Ali SF, Dervishi E, Xu Y, Li ZR, Casciano D, Biris AS (2010) Cytotoxicity effects of graphene and single-wall carbon nanotubes in neural phaeochromocytoma-derived PC12 cells. ACS Nano 4:3181–3186

Zhou Y, Bao QL, Tang LAL, Zhong YL, Loh KP (2009) Hydrothermal dehydration for the "green" reduction of exfoliated graphene oxide to graphene and demonstration of tunable optical limiting properties. Chem Mater 21:2950–2956